SAR Methods and Applications for Cryosphere Monitoring

Part 1

Helmut Rott
ENVEO IT, Innsbruck
& University of Innsbruck, Austria

ESA/CONAE SAR Course, 12-17 November 2018, Buenos Aires

Components of the Cryosphere and their Time Scales

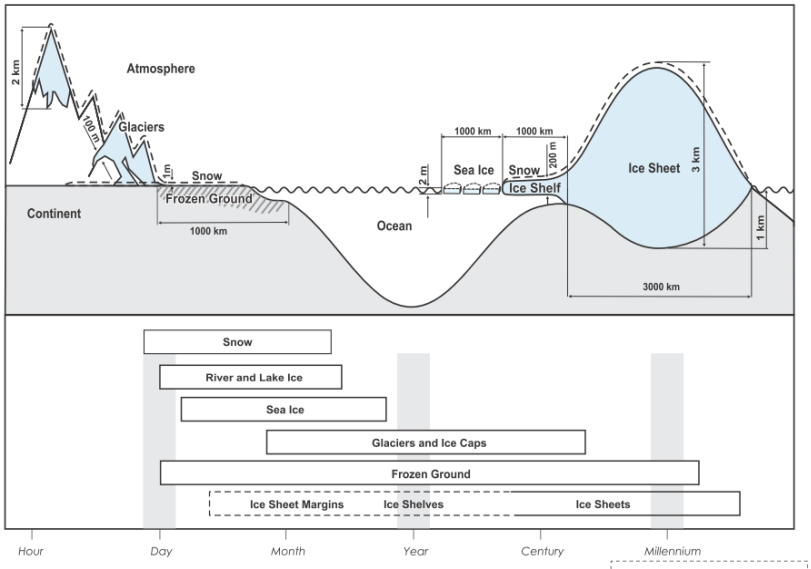

Lemke et al., 2007

Contents of the Lecture

1. Radar Signal Propagation in Snow and Ice
   - Snow Morphology
   - Dielectric Properties and Signal Penetration
   - Radar Backscatter Signatures
   - Sea Ice Backscatter Signatures
2. SAR Application for Snow Cover Monitoring
   - Snowmelt Area Mapping
   - Experimental Study on Retrieval of Snow Mass (SWE)
   - Repeat-pass InSAR Retrieval of SWE
   - Snowmelt Runoff Modelling

Snow Properties after Melt/Freeze Metamorphism

AlpSAR Test Site Leutasch, 22 Feb 2013
1100 m a.s.l.

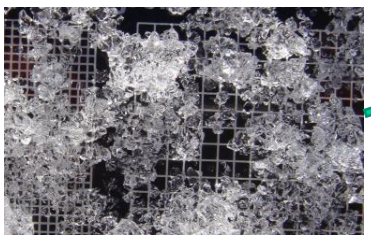

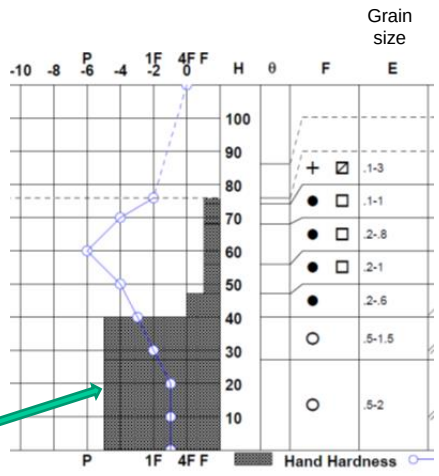

Grain clusters after several cycles of melt/freeze metamorphism

Rotmoos - Temperature Gradient Metamorphism

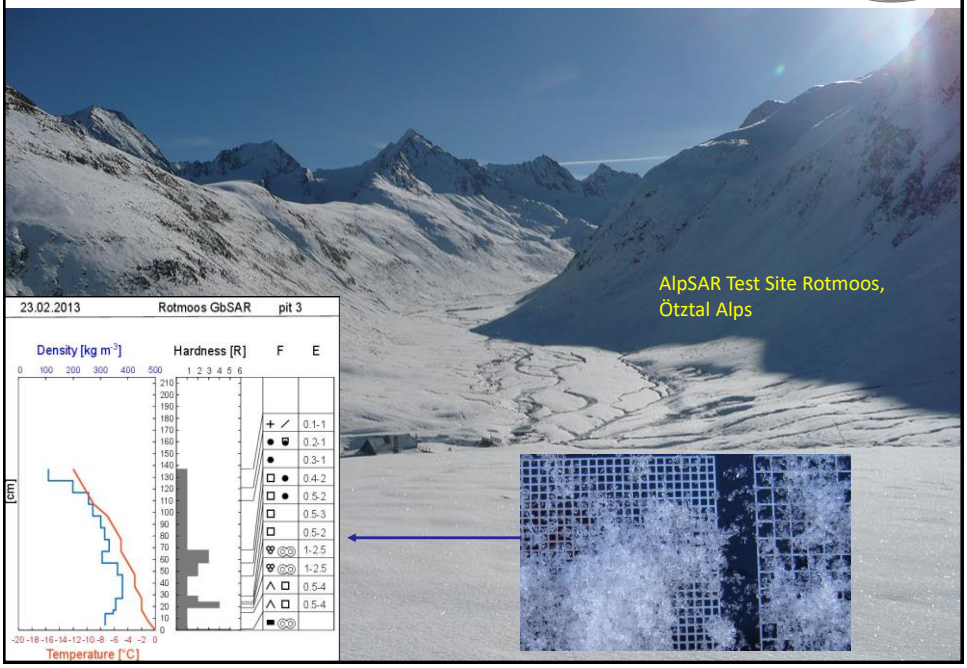

Glacier - Winter Snow on Frozen Firn and Ice

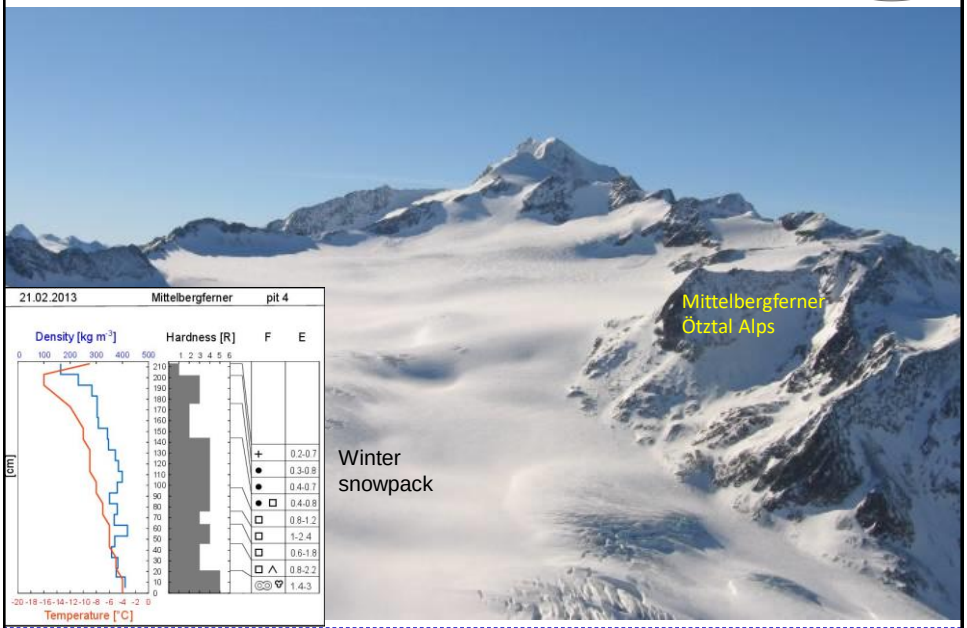

Microwave Permittivity of Ice and Snow

Ice:

ε‘ = 3.15

ε“ = 0.001 to 0.0001 f (v, T)

ν_0 (-0.1°C) = 7.3 KHz

Dry snow:

ε‘ =1.0 + 1.7 ρ + 0.7 ρ^2

Wet snow:

ε‘ = ε‘ (dry) + Δ ε

Δε = 0.23 V_w / [1 - i(ν/ ν_0)]

V_w [% volume]

ν_0 relaxation frequency for wet snow (ca. 10 GHz)

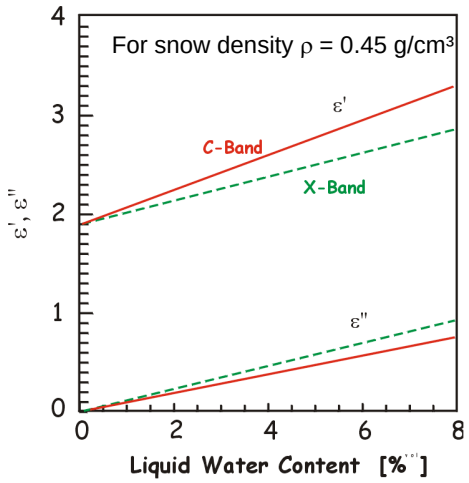

$$d_p = \frac{1}{k_a} = \frac{\lambda_o}{2\pi}\frac{\sqrt{\varepsilon'}}{\varepsilon''}$$

Penetration depth for lossy medium, ε‘ >> ε“

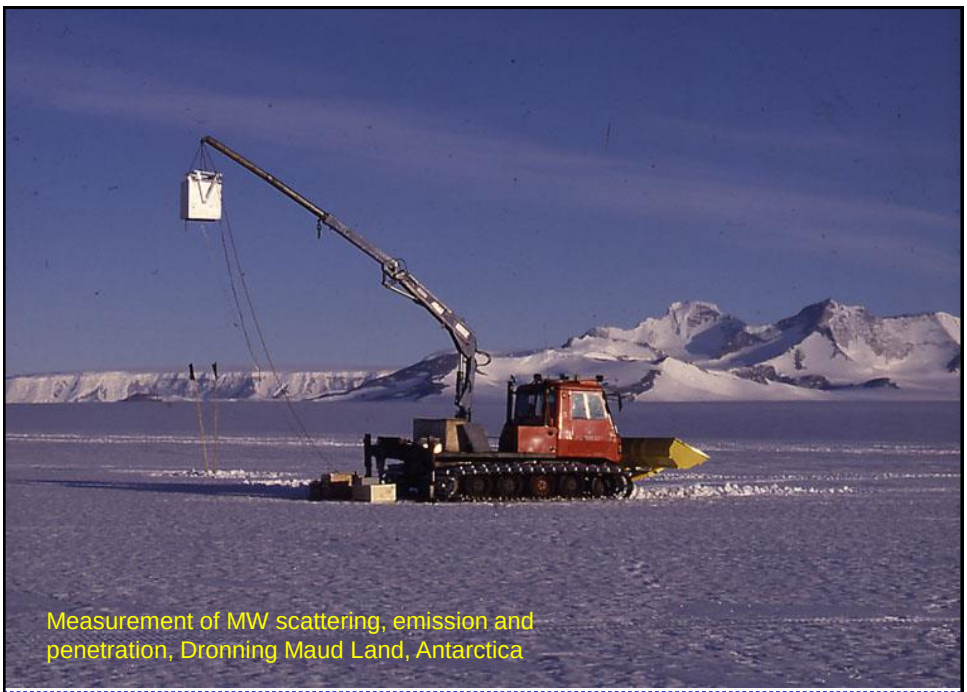

Measurement of MW scattering, emission and penetration, Dronning Maud Land, Antarctica

Microwave Penetration Depth in Dry Snow

$$d_p = \frac{1}{k_e} = \frac{1}{k_s + k_a}$$

k_a and k_s [m^{-1}]
absorption & scattering coefficient.

Dry snow: $k_s > k_a$

Data base

- *Alpine snowpack (Mätzler, 1987)*
  Field measurements
- *Antarctic snow (Rott, 1993)*
  Field measurements
- *Retrieved by inversion of satellite MW radiometry, Antarctic* Plateau (Rott, 1993)

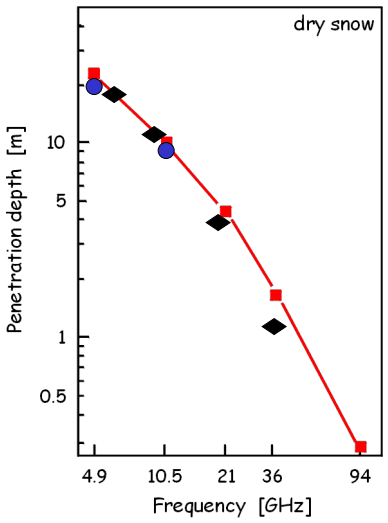

Microwave Penetration Depth in Wet Snow

Microwave permittivity of water

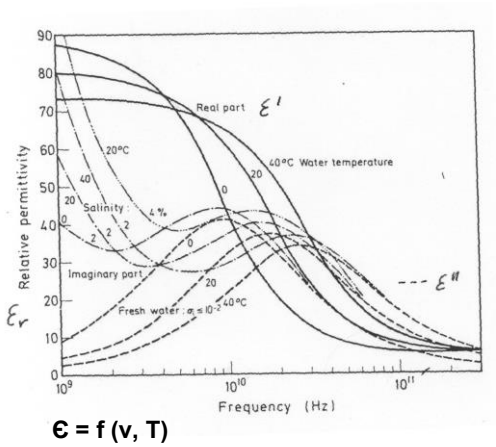

Є = f (v, T)

ν_0 (0°C) = 8.84 GHz

Debye Relaxation

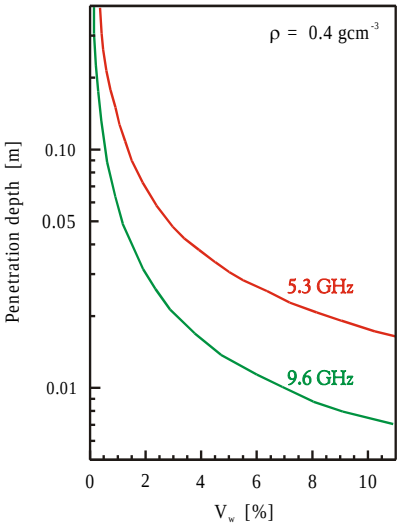

V_w volumetric liquid water content

Radar Signal Propagation for Snow over Ground

1st order radiative transfer (RT) formulation for singe layer

$$\sigma^\circ = \sigma^\circ_{as} + \gamma^2_{as}\left[(\sigma^\circ_v / 2k_e)(1 - t'^2_s)\cos\theta + \sigma^\circ_g t'_s\right]$$

Snow volume contribution Ground

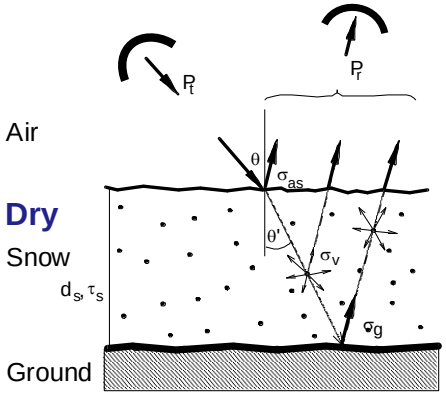

σ° = backscattering cross section

σ°_{as} = backscat at air/snow interface

γ_{as} = transmission coefficient air/snow

σ°_v = volume backscattering coeff.

σ°_g = backscatt. coeff. of ground

$k_e = k_s + k_a$ volume extinction coeff.

t_s = transmissivity of snow layer

$t'_s = \exp(-k_e d_s/\cos\theta')$

d_s = snow depth

$\omega_0 = k_s / k_e$ single scattering albedo

Radar Signal Contributions for Dry Snow over Ground

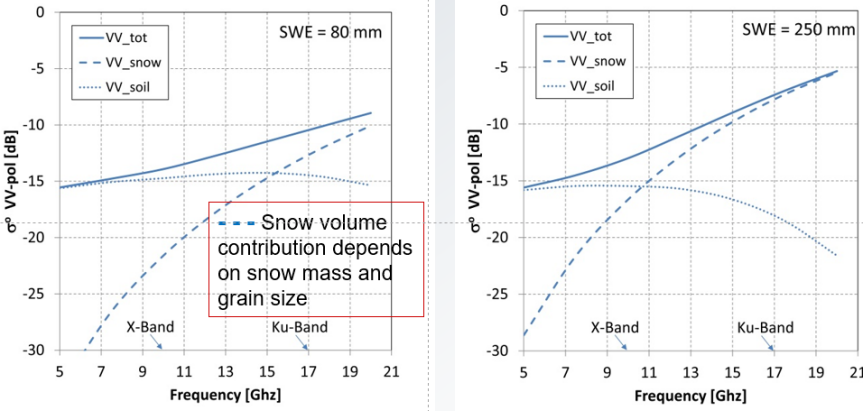

Backscatter coefficients σ°, VV polarizations, $\theta = 40^\circ$
Computed by dense medium Radiative Transfer model; grain size ∅ 1.0 mm
For snow mass (SWE): 80 mm (40 cm snow depth) and 250 mm (120 cm d_s)

Backscatter Sensitivity to Snow Mass– Impact of Grain Size

RT simulation for backscatter of dry snow over ground

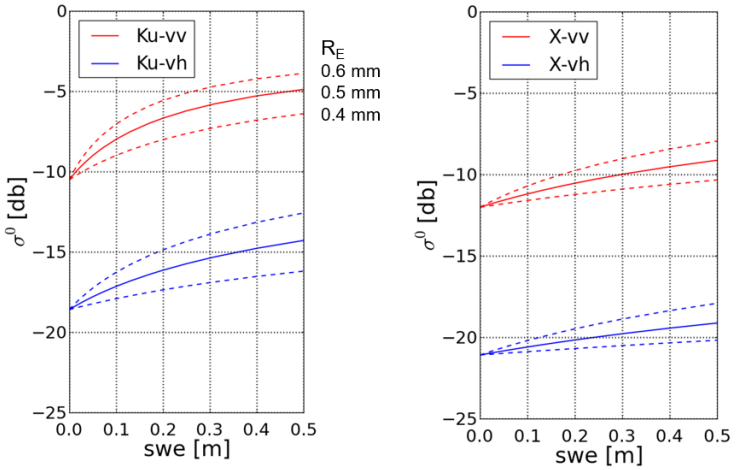

Main parameters for backscatter intensity: SWE and effective grain size (eGS)

eGS – parameterization for backscatter efficiency of the snow volume

Complex Structure of Natural Snow Packs

Multiple layers

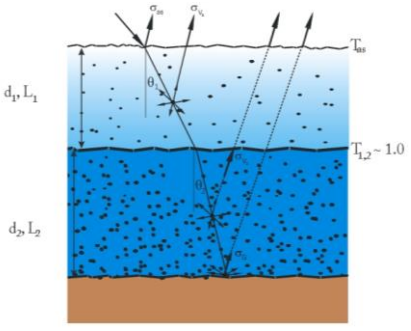

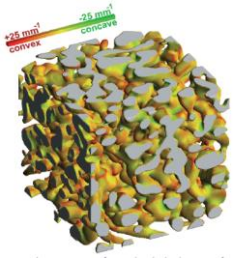

Snow cover is a *sintered medium*.

For backscatter modelling the scattering efficiency is parameterized by effective grain size (has different scattering phase function).

Multiple Scattering

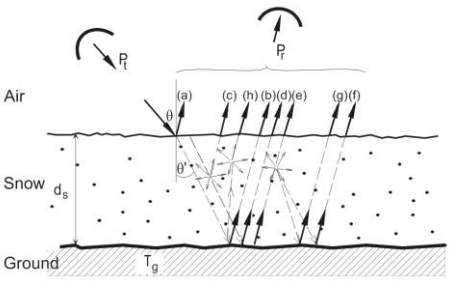

X-Band Backscatter Signatures of Snow

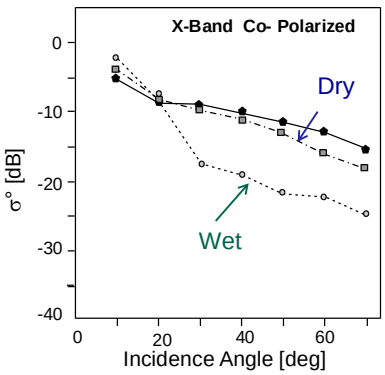

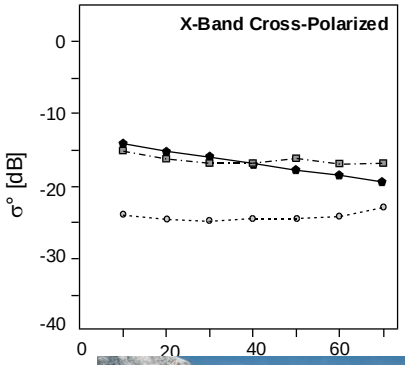

◆ snow-free (meadow)

☐ dry snow (fine-grained) – low loss medium

○ wet snow ⟶ low σ° (absorption)

Measurements in Alpine valley (*Leutasch*)

C-Band Backscatter Signatures of Snow

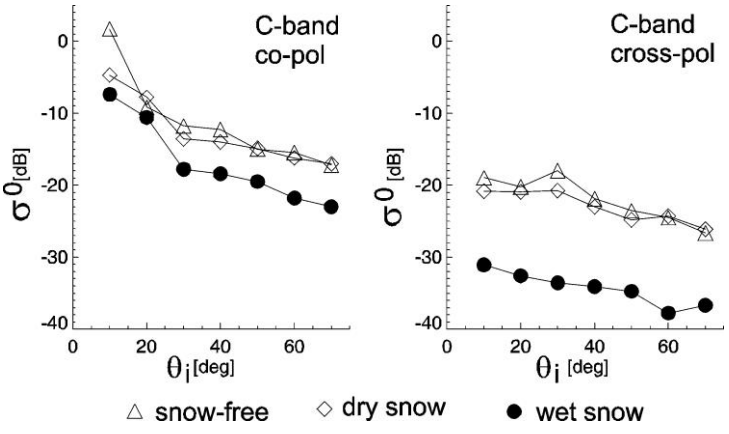

Measurements in Alpine valley (*Leutasch*)

Main Factors for Backscattering of Snow, Ku- to L-Band

WET SNOW ***Dominant Scattering Mechanism:*** **Surface Scattering**

• Liquid water content	*dominant factor*
• Surface roughness	*important*
• Grain size	*relevant for high SAR frequencies*

DRY SEASONAL SNOW: Scattering in the Volume and/or at Lower Interface

• σ° of medium below snow	*dominating for seasonal snow at f<~10 GHz*
• Grain size	important *for f>~10 GHz*
• *Snow Mass (snow water equivalent, SWE)* →	*Little sensitivity of σ° at X- to L-band; Ku-band sensitive to SWE, but ambiguity with grain size*

REFROZEN SNOW (***e.g. firn area on glaciers***): **Volume Scattering**

- Volume inhomogeneities (grains, grain clusters, ice lenses, ice pipes, ..)
- Internal interfaces between snow layers of different density

Main Factors for Backscattering of Snow, Ku- to L-Band

WET SNOW ***Dominant Scattering Mechanism:*** **Surface Scattering**

• Liquid water content	*dominant factor*
• Surface roughness	*important*
• Grain size	*relevant for high SAR frequencies*

DRY SEASONAL SNOW: Scattering in the Volume and/or at Lower Interface

• σ° of medium below snow	*dominating for seasonal snow at f<~10 GHz*
• Grain size	important *for f>~10 GHz*
• *Snow Mass (snow water equivalent, SWE)* →	*Little sensitivity of σ° at X- to L-band; Ku-band sensitive to SWE, but ambiguity with grain size*

REFROZEN SNOW (***e.g. firn area on glaciers***): **Volume Scattering**

- Volume inhomogeneities (grains, grain clusters, ice lenses, ice pipes, ..)
- Internal interfaces between snow layers of different density

Dielectric Properties of Sea Ice

Penetration depth
for different ice types

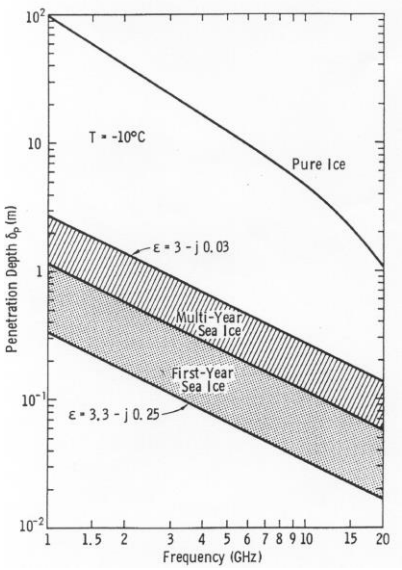

Strong Variability of ε" in dependence of brine content

Sea ice is a heterogeneous mixture of pure ice crystals, gas (air) bubbles and brine pockets in either liquid or solid forms

→ Absorption losses dominate in young sea ice

→ Scattering losses dominate in multi-year ice

Salinity and Structure of First-Year Sea Ice

Granular sea ice

Fig. Geophys. Inst. Univ. Alaska

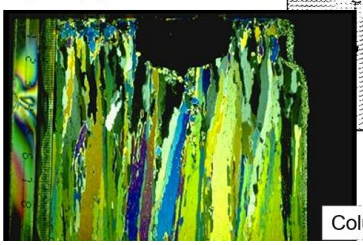

Columnar sea ice.

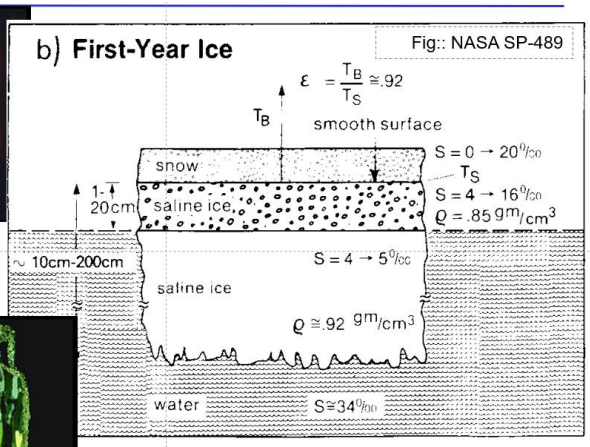

High brine content – high absorption / emission coefficient

Salinity and Structure of Multi-Year Sea Ice

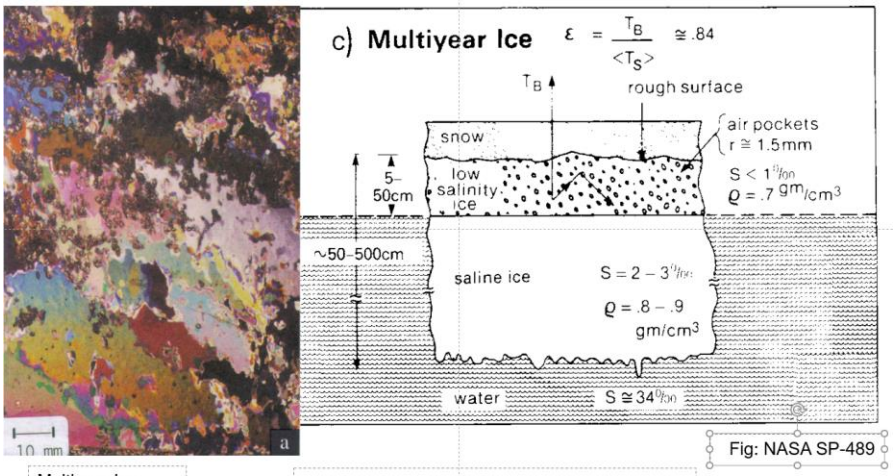

Fig: NASA SP-489

Multiyear Ice, (Shokr, 1991)

Losses dominated by **volume scattering** – air bubbles, grain clusters

L-band and C-Band Discrimination of Sea Ice vs. Water

Winter conditions

L-band VV

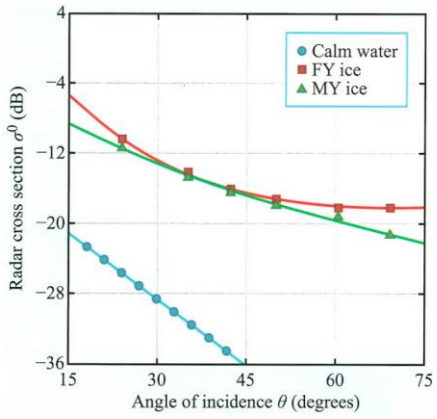

C-band HH

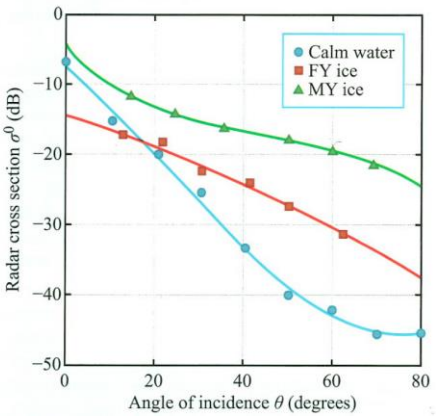

Ref: Ulaby and Long, 2015

Contrast between ICE Types at Different SAR Frequencies

Winter conditions

First year thin vs. thick

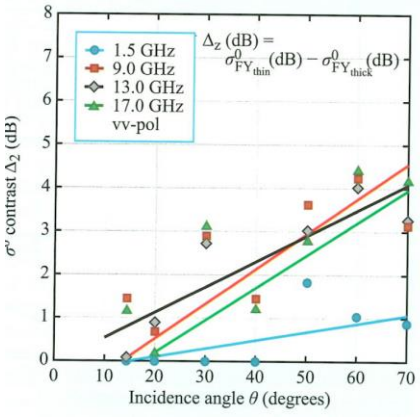

Multi-year vs. first year

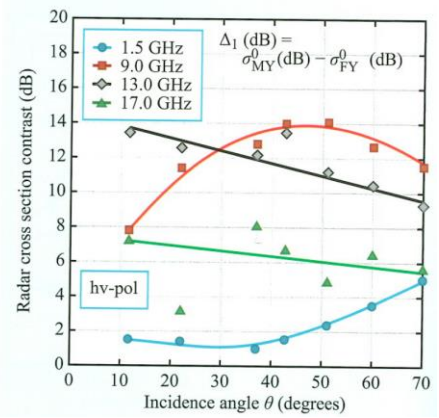

Ref: Ulaby and Long, 2015

Sea Ice Deformation Features in L-Band and C-Band

EMAC airborne campaign Gulf of Bothnia, March 1995

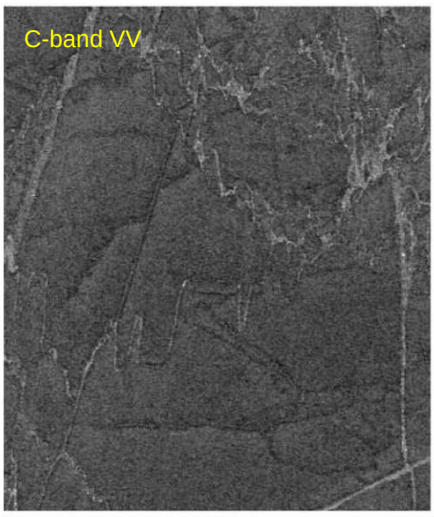

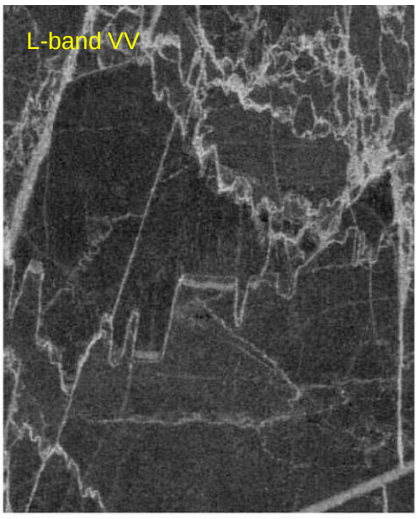

Ref: Dierking and Dall, 2017

L-Band Sensitivity on Thickness of Thin Sea Ice

Thin sea ice retrieval from ALOS/PALSAR, L-band HH *Ref: Toyota et al. 2011*

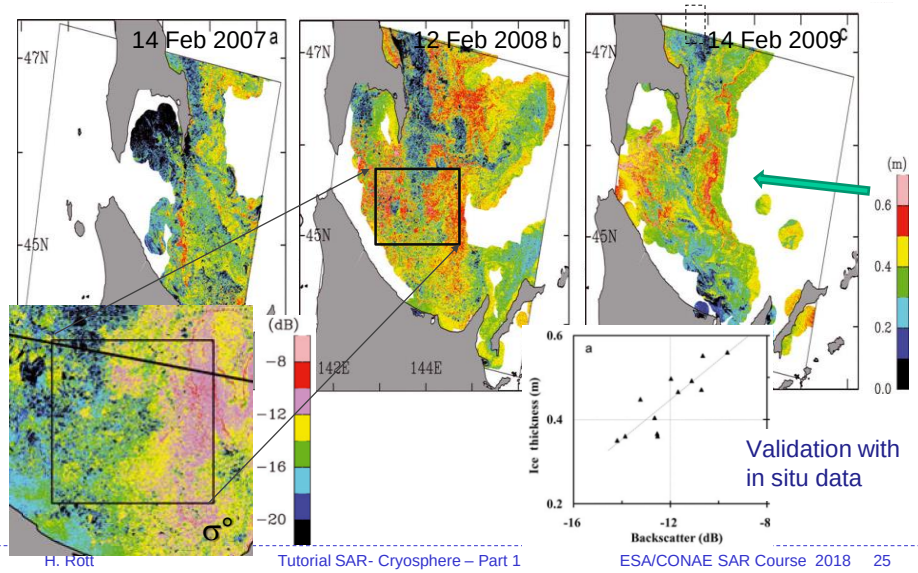

SAR Algorithm for Retrieval of Snowmelt Area

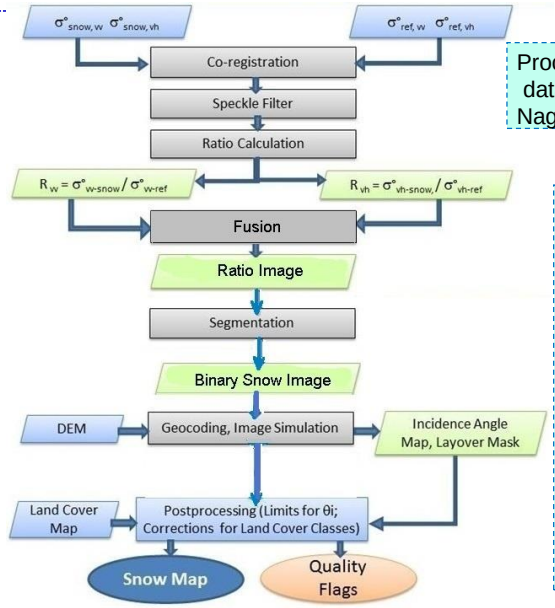

Processing line for Sentinel-1 IW mode data (C-band, VV & VH polarization) Nagler et al., 2016

Basic Concept:

- Uses C-band or X-band SAR data
- Exploits the contrast of backscatter between wet snow and snow-free (or dry snow) reference conditions
- Applies the backscatter ratio ($\sigma^\circ_{wetsnow}/\sigma^\circ_{reference}$) to compensate for topographic effects, **Change detection**
- Applies a segmentation procedure for separating the two surface types in σ°- ratio images

Impact of SAR Geometry in Mountainous Terrain

Across track geometry

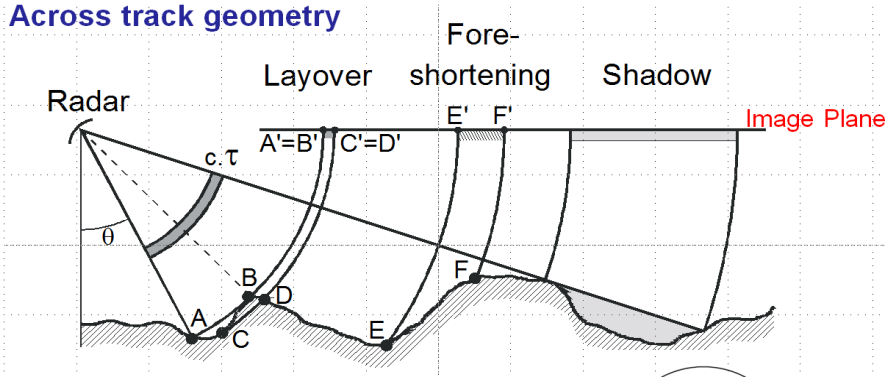

Topographic distortion depends on local incidence angle

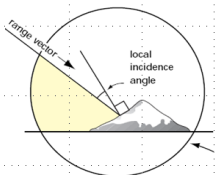

Surface resolution across track: $\Delta r = c\tau/(2\sin\theta_{inc})$

Impact of Different Look Angles on Terrain-related Deformation

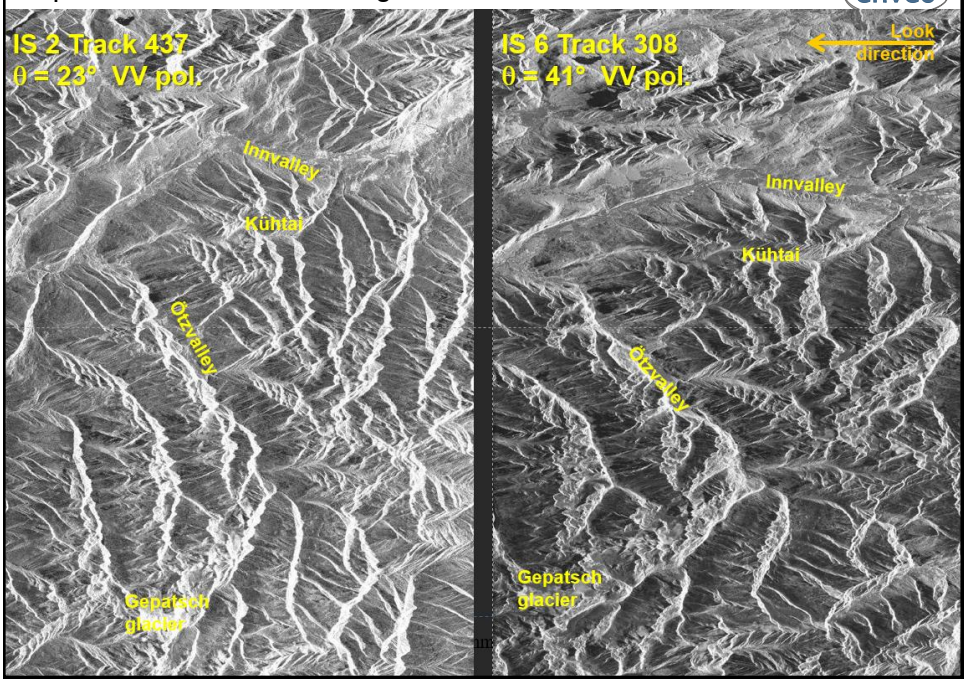

Sentinel-1 Backscatter Signatures of Wet Snow

Backscatter ratio (wet snow vs. snow-free surfaces) Sentinel-1 VV- and VH-polarized channels in dependence of local incidence angle, θ, Ötztal Alps

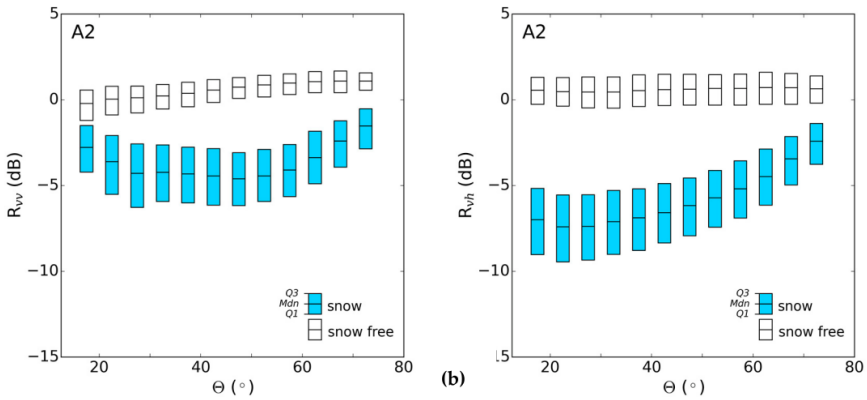

Cross-pol provides better discrimination at low off-nadir angles

Snowmelt Area by Sentinel-1 SAR IW Mode Data

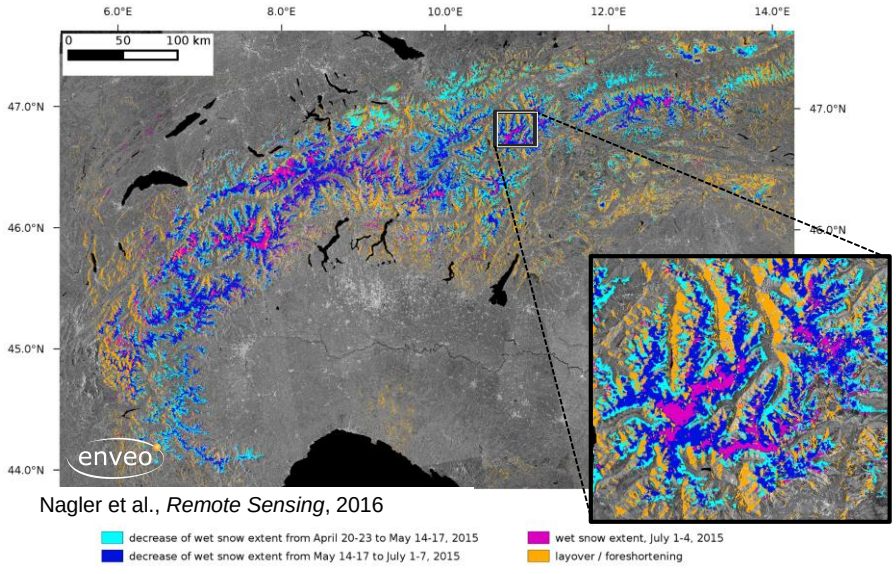

Nagler et al., *Remote Sensing*, 2016

Snowmelt Area by Sentinel-1 SAR IW Mode Data

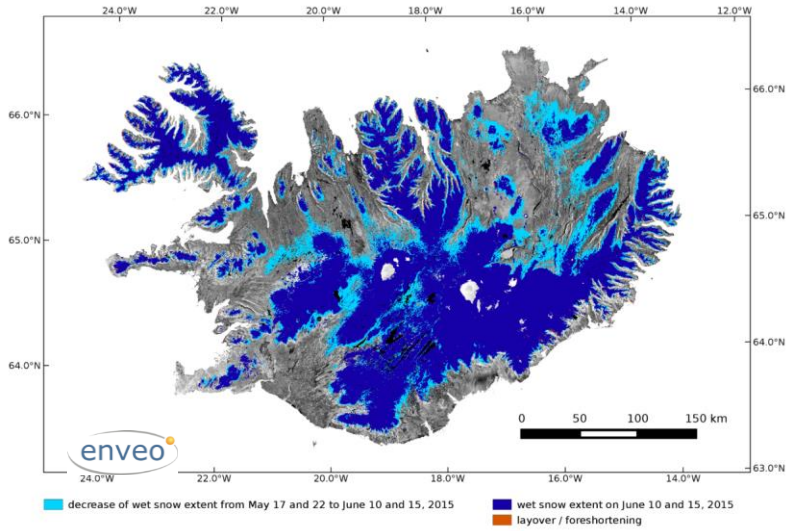

Snowmelt Area by Sentinel-1 SAR IW Mode Data

Snow map Tröllaskagi Peninsula, Iceland

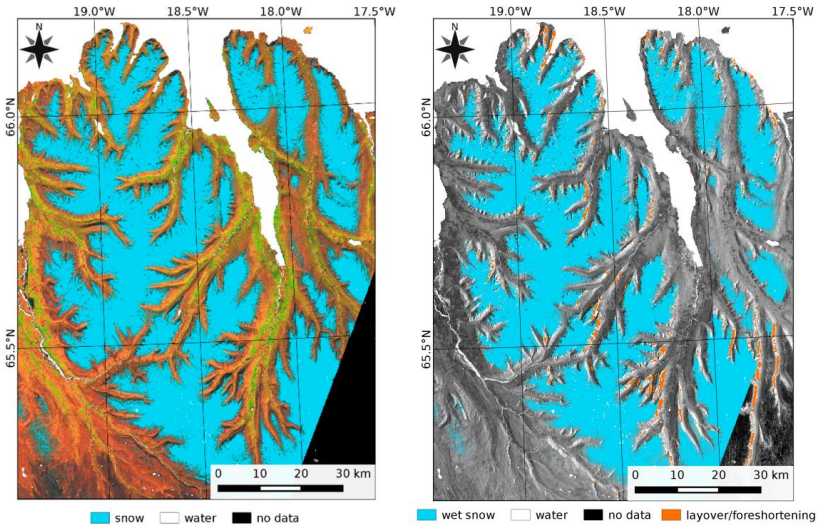

Landsat, 27 June 2015

Sentinel-1, 26 June 2015

Wet Snow Extent on Glaciers, from TerraSAR-X Data

G – Gepatsch Glacier
H – Hintereis Glacier
(Ötztal)

Red – wet snow; yellow - layover

25 Dec 2010

10 July 2009

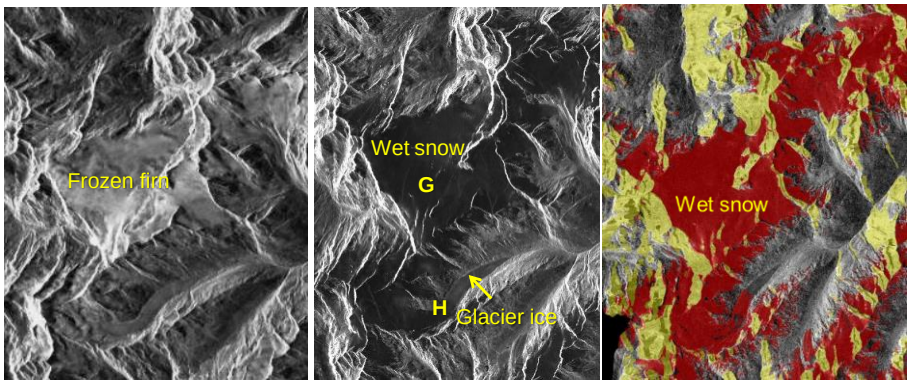

NoSREx campaign towards Ku-& X-Band SAR for SWE

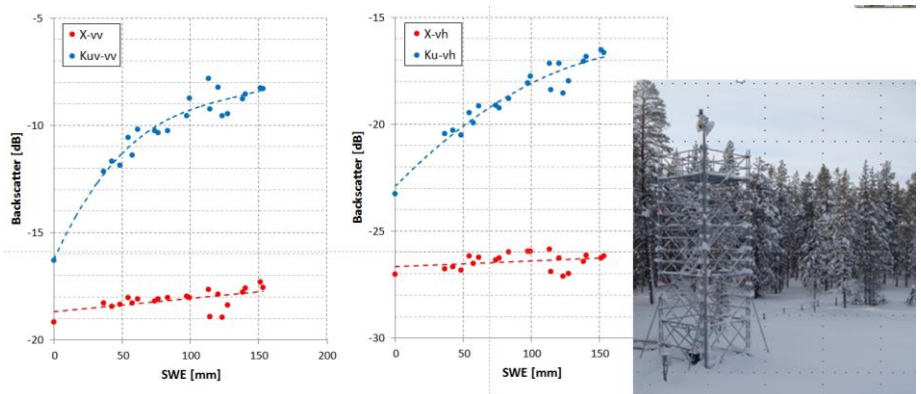

SnowScat σ° (dB) at Ku-band (16.7 GHz) and X-band (10.2 GHz), θ = 40° winter 2010/11, versus SWE in snow pits, Sodankylä, Finland (NoSREx-2).

Phase-A studies for ESA Earth Explorer Candidate CoReH2O, *Rott et al., 2009*

NoSREx campaign towards Ku-& X-Band SAR for SWE

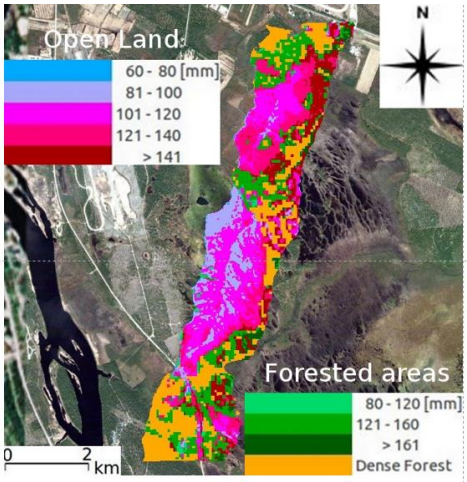

SWE map, derived from SnowSAR data, Sodankylä, 15/03/2011

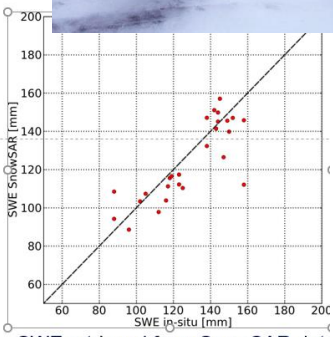

SWE retrieved from SnowSAR data vs. in situ point measurements

SWE_{obs} – SWE_{ret} = -5 mm

Stand. error : 12.7 mm

Repeat-Pass InSAR for Retrieval of Snow Mass

Basic Approach:

- Differential processing of repeat-pass InSAR data to obtain ϕ_{snow}
- Propagation path length through dry snow is related to SWE

Total interferometric phase difference: $\phi = \phi_{flat} + \phi_{topo} + \phi_{atm} + \phi_{snow}$

Phase delay in dry snow pack: *Guneriussen et al., 2001*

$$\Delta\phi_{snow} = -2k\ \Delta d_s \left(\cos\theta_i - \sqrt{\varepsilon - \sin\theta_i^2}\right)$$

k = 2π/λ

$$\Delta\phi_{snow} = -2k\Delta d_s \left(\cos\theta - \sqrt{1 + 1.56\ \rho_s\ \sin\theta^2}\right)$$

For incidence angles θ < ca. 40°:

$$\Delta\phi_{snow} = 4\pi/\lambda_0 \left(Const._{\lambda,\theta}\ \Delta SWE\right)$$

$\Delta\phi_{snow}$ = 2π ⇒ Δ SWE = 3.2 cm (C-band)

(θ=23°) ⇒ Δ SWE = 14 cm (L-band)

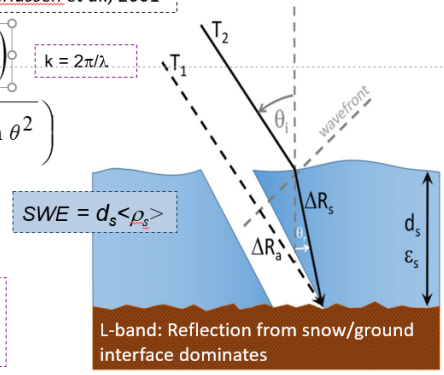

Impact of Frequency for InSAR SWE Retrieval

The InSAR SWE retrieval algorithm is based on **dominating return from snow/ground interface**. Effects caused by scattering contributions from snow volume are neglected ⇒ **Preference for long wavelength**.

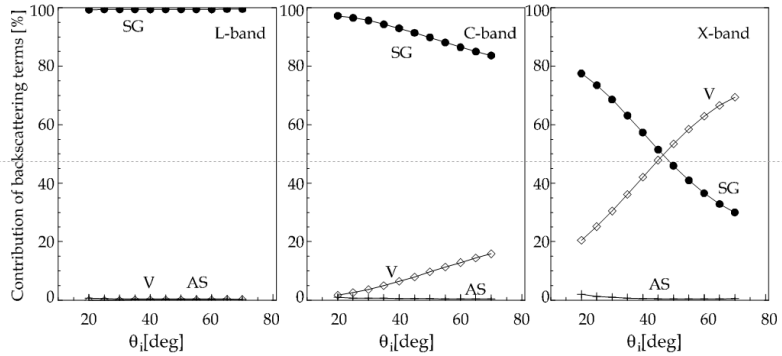

Relative contributions of the main scattering terms for dry snow of 2.5 m depth and R_E = 0.5 mm over soil at L-, C- and X-band. AS - scattering from the air/snow interface, SG - scattering from the snow/ground interface, V - volume scattering

Phase Sensitivity to SWE and 2π Ambiguity

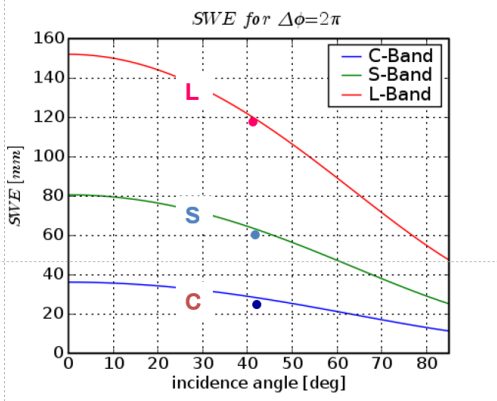

Relation SWE ↔ Snow Depth, for Δϕ=2π, θ=40°:

	SWE	SD(100 kg m^{-3})	SD(300 kg m^{-3})
L-Band:	120 mm	1.20 m	0.40 m
C-Band:	28 mm	0.28 m	0.09 m

Impact of refraction on phase

Example for L-Band with SWE = 20 mm

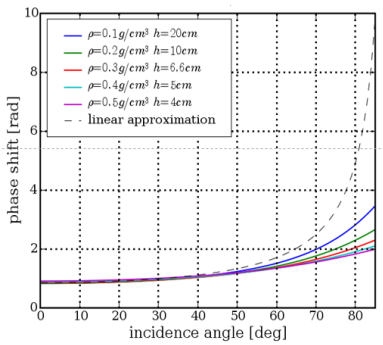

Corrections for refractions (density) needed at θ > 40 deg.

Impact of Temporal Decorrelation on Coherence

Model calculations for temporal decorrelation due to snowfall or snow drift causing changes in phase delay at sub-pixel scale

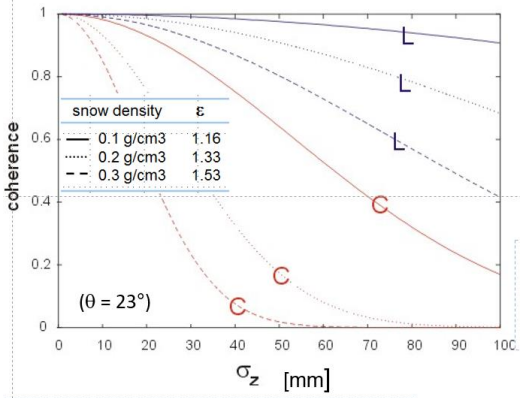

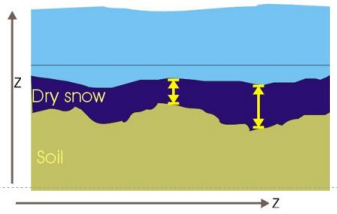

← Estimate for decorrelation, assuming variations of phase delay at sub-pixel scale for snow above rough surface with Gaussian distribution for σ_z

σ_z standard deviation of phase length within pixel due to snow fall, for distributed scatterer

$$|\gamma_{temporal}| = \exp\left[-\frac{1}{2}\left(\frac{4\pi}{\lambda_0}\right)^2 \sigma_z^2 \left(\cos\theta_i - \sqrt{\varepsilon - \sin\theta_i^2}\right)^2\right]$$

Temporal Change of InSAR Phase & Relation to SWE

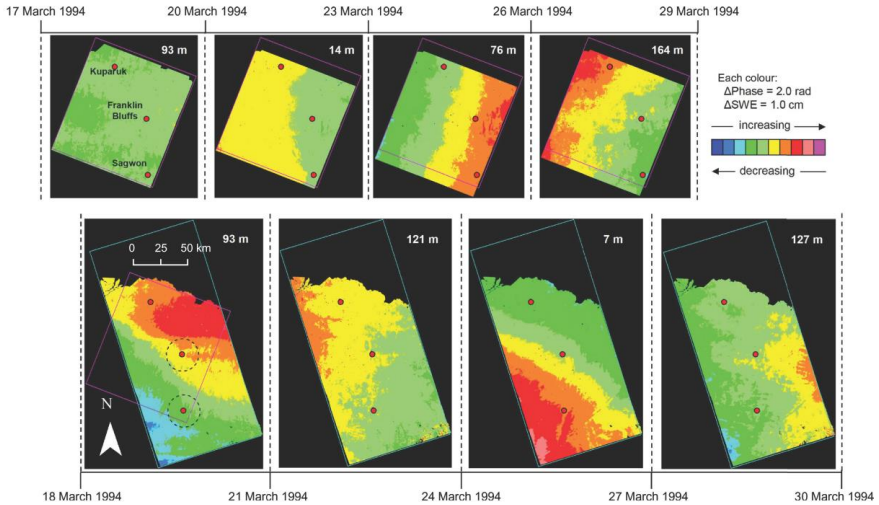

Alaska North Slope, 3-day ERS-1 repeat pass
Changes of SWE due to snowfall and wind erosion/deposition

Deeb et al., 2011

Field Experiment with Ground-based InSAR for SWE Retrieval

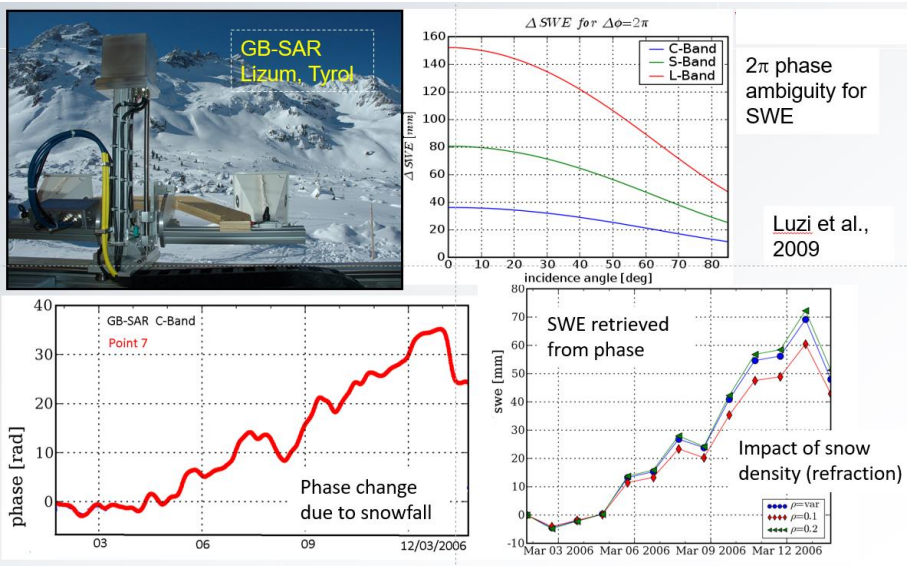

Processing System for Snowmelt Runoff Forecasting

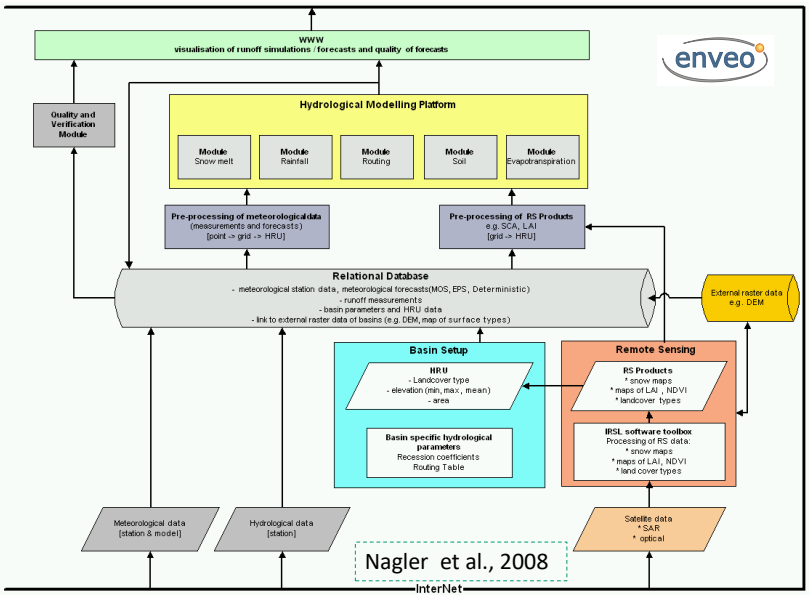

Short-term Runoff Forecasting – Mesocsale Meteo Data Input

Temperature

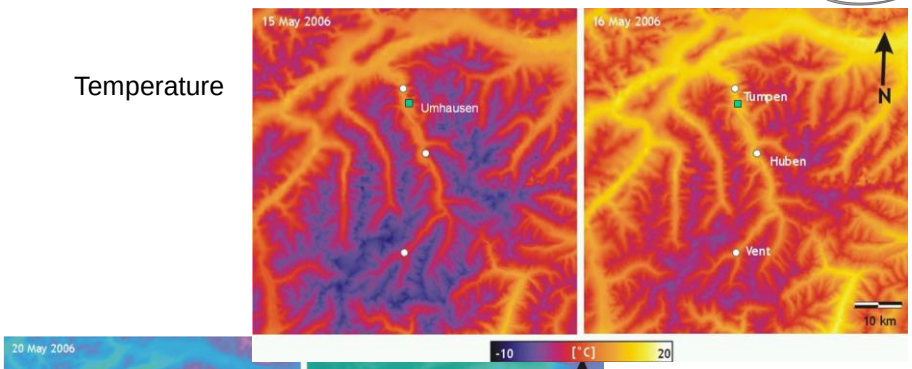

Precipitation

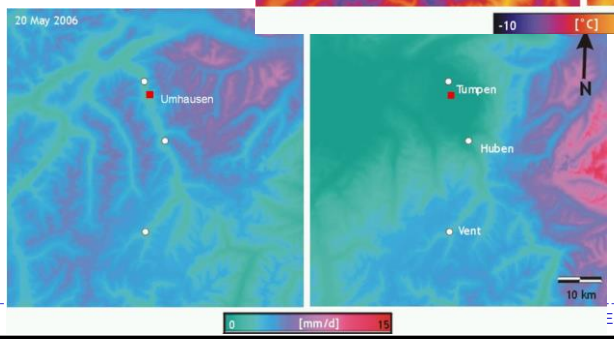

Snow-covered Area - ASAR Map of Snowmelt Area

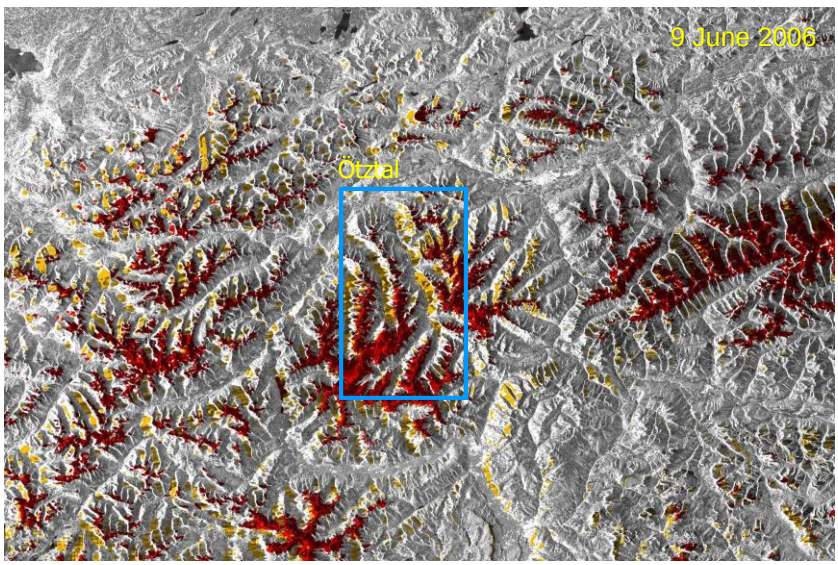

Basin-Setup Ötztal

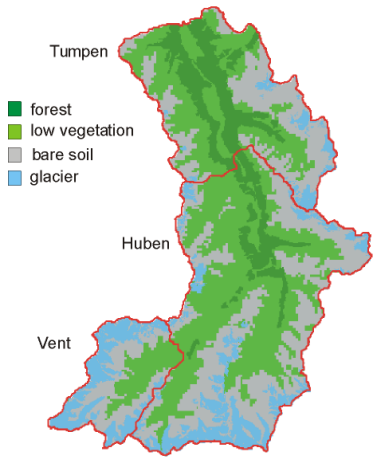

(a)

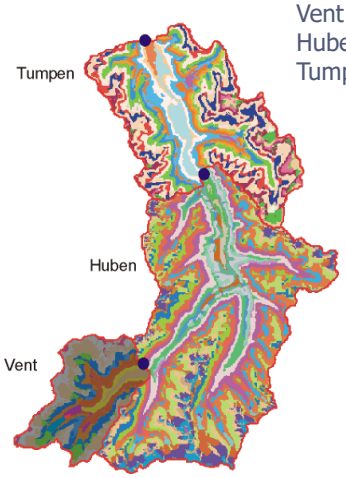

(b)

No of HRUs
Vent - 17
Huben - 27
Tumpen - 28

Real-Time Runoff Forecast during Snowmelt Period

Daily runoff forecasts for 1 to 6 days (colour coded)

Sub-basin Vent

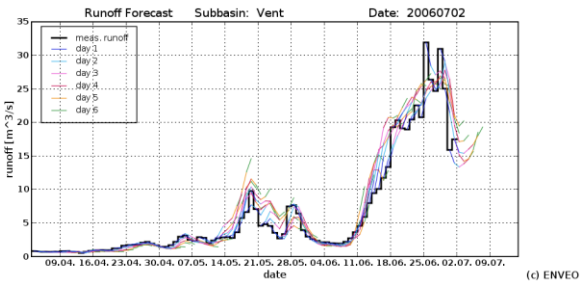

Ötztal main basin

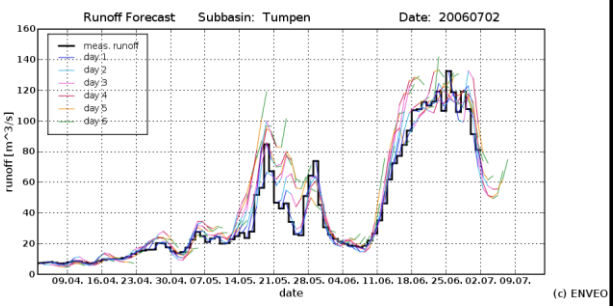

Main uncertainties related to rainfall forecast

References

- Deeb, E.J., R.R. Forster, D.L. Kane. 2011. Monitoring snowpack evolution using interferometric synthetic aperture radar on the North Slope of Alaska. Int. J. Rem. Sens, 32(14), 3985-4003.
- Guneriussen, T., Hogda, K.A., Johnson, H., Lauknes, I. 2001. InSAR for estimating changes in snow water equivalent of dry snow, *IEEE Trans. Geosc. Rem. Sens*. 39(10), 2101-2108.
- Luzi, G., Noferini, L., Mecatti, D. et al. 2009. Using a ground-based SAR interferometer and a terrestrial laser scanner to monitor snow. IEEE *Trans. Geosc. Rem. Sens*. 74(2) 382-393.
- Nagler T., H. Rott , P. Malcher, F. Müller. 2008. Assimilation of Meteorological and Remote Sensing Data for Snowmelt Runoff Forecasting. Rem. Sens. Environment, 112, 1408-1420.
- Nagler T. and H. Rott, 2000. Retrieval of wet snow by means of multitemporal SAR data. *IEEE Trans. Geosc. Rem. Sens.,* 38, 754-765.
- Nagler, T., Rott, H., Ripper, E., et al. 2016. Advancements for Snowmelt Monitoring by Means of Sentinel-1 SAR. *Remote Sens.,* 8(4), 348; doi: 10.3390/rs8040348
- Rott, H., Yueh, S.H., Cline, D.W, C. Duguay, R. Essery, C. Haas, F. Hélière, M. Kern, G. Macelloni, E. Malnes, T. Nagler, J. Pulliainen, H. Rebhan, A. Thompson. 2010. Cold Regions Hydrology High-resolution Observatory for Snow and Cold Land Processes. Proceedings of the IEEE, 98(5), 752 – 765.
- Toyota, T., Ono, S., Cho, K. and K.I. Ohshima. 2011. Retrieval of sea-ice thickness distribution in the Sea of Okhotsk from ALOS/PALSAR backscatter data. Ann. Glac. 52 (57), 177 – 184.
- Ulaby, F.T. and D.G. Long. 2015. Microwave and Radar Remote Sensing. Artech House , Boston, London.